Journal of Environmental Science and Engineering A 2 (2013) 744-752
Formerly part of Journal of Environmental Science and Engineering, ISSN 1934-8932

Iron Activation of Natural Aluminosilicates to Remove Arsenic from Groundwater

Irma Lía Botto[1], María José González[1, 2], Delia Gazzolli[3] and Edgardo Luís Soto[4]

1. CEQUINOR-CONICET (Centre for Inorganic Chemistry), University of La Plata, La Plata 1900, Argentina

2. INREMI-CICPBA (Institute of Mineral Resources), University of La Plata, La Plata 1900, Argentina

3. Department of Chemistry, University of Roma La Sapienza, Rome 00185, Italia

4. Multipurpose Pilot Plant (PLAPIMU-CICPBA), University of La Plata, Gonnet 1897, Argentina

Received: November 11, 2013 / Accepted: December 17, 2013 / Published: December 20, 2013.

Abstract: Low-cost adsorbents constituted by Fe-modified-aluminosilicates (laminar and zeolite type minerals) were developed and characterized to be used in the arsenic removal from groundwater. Iron activation was carried out "in situ" by the synthesis and deposition of mesoporous ferrihydrite. Natural iron-rich aluminosilicate was used as reference. All samples were characterized by X-ray diffraction, Raman spectroscopy, BET N_2-adsorption, SEM-EDS microscopy and ICP chemical analysis. Experimental results of arsenic sorption showed that iron-poor raw materials were not active, unlike iron activated samples. The iron loading in all activated samples was below 5% (expressed as Fe_2O_3), whereas the removal capacity of these samples reaches between 200-700 μg of As by g of adsorbent, after reusing between 17 cycles and 70 cycles up to adsorbent saturation. Differences can be associated to mineral structure and to the surface charge modification by iron deposition, affecting the attraction of the As-oxoanion. On the basis of low-cost raw materials, the easy chemical process for activation shows that these materials are potentially attractive for As(V) removal. Likewise, the activation of clay minerals, with natural high content of iron, seems to be a good strategy to enhance the arsenic adsorption ability and consequently the useful life of the adsorbent.

Key words: Arsenic removal, iron activation, aluminosilicates.

1. Introduction

As (Arsenic) is a very toxic element, observed in some groundwater bodies at levels above those suggested by the WHO (10 $\mu g \cdot L^{-1}$). The impact of natural As toxicity of groundwater hydrologic system is the main responsible for serious human health problems, predominantly the pathology known as CERHA (chronic endemic regional Hydroarsenicism) [1, 2]. Some regions of the world, prevalently southeast and east Asia as well as north and south America (e.g. Argentina, Bolivia, Chile, Canada, USA), west Africa and coastal Australia, are particularly affected [3]. So, both the drinkable water scarcity as well as the lowering of the as standards from 50 $\mu g \cdot L^{-1}$ to 10 $\mu g\ L^{-1}$ by regulatory agencies and advisory bodies (USEPA; WHO) are critical for survival of several million people. This situation has raised the need to take up urgent mitigation actions to reduce the health risk to consume water with arsenic. In this sense, different types of technological strategies to remove the contaminant are reported [4]. However, the As adsorption by using synthetic and natural low cost products appears as one effective and economic solution, particularly promising for areas of low population density and low income [5-8]. The removal by this technique is usually carried out in batch, column or bed reactors by using preferably iron and aluminum oxide species as adsorbents [9]. Several synthetic and mineral species such as hematite, goethite, siderite, as well as laterites and other

Corresponding author: Irma Lía Botto, Ph.D., emeritus professor, main research fields: inorganic chemistry, characterization of natural and synthetic adsorbents. E-mail: botto@quimica.unlp.edu.ar.

chemical combinations (red-mud, iron-coated sand, etc.) are extensively reported in literature [7-14].

In Argentina, arsenical groundwater is found in the great Chaco-Pampean area (more than 10^6 km^2), affecting particularly cities and small populations where it is not possible the access to drinkable water [2]. In the aquifers, the "in situ" adsorption by a Fe-Al silicate matrix is one of the arsenic mobility control parameters. Hence, both the acute health effects of drinking contaminated waters and the abundance of aluminosilicate mineral resources in our country were enough motivations to develop a technological process based on the use of iron-rich natural clay as adsorbent. This procedure was implemented in rural areas of some Argentinean affected regions [15]. According to the designed process, more than 4×10^5 L of water, originally with 220 $\mu g \cdot L^{-1}$ As, were processed in batch by using an iron rich clay/water ratio of 1/10, in pilot plants installed in rural zones of Buenos Aires Province, by water production with an arsenic value < 10 $\mu g \cdot L^{-1}$.

In the search of other low-cost adsorbents for the production of drinkable water, a series of materials were tested at laboratory scale. Natural low-iron aluminosilicates, such as zeolite (clinoptilolite) as well as clay minerals 2:1 and 1:1 type (containing P (pyrophyllite) and K (kaolinite) as predominant phases), were chemically modified to set the iron content suitable for the arsenic removal process. The study was done with the aid of Jar Test equipment and physicochemical techniques such as XRD (X-Ray diffraction), ICP-AES (inductively coupled plasma atomic emission spectroscopy) chemical analysis, SEM-EDS (scanning electron microscopy), BET (Braunauer, Emmet & Teller) surface area measurements and Raman spectroscopy.

2. Materials and Methods

2.1 Chemical Characterization

Raw minerals with low iron content such as Z (zeolite clinoptilolite), P and K clays from Argentinean deposits were characterized and employed in the study of arsenate adsorption. A Fe-rich clay mineral (~50% Fe_2O_3), identified as FC, was used as Ref. [15]. Particle fractions with sizes lower than 1 mm were used for As adsorption tests.

The chemical modification was performed according to the Schwertmann and Cornell technique [16]. The method consists in the combination of 100 g of aluminosilicate with 20 g of $FeCl_3 \cdot 6H_2O$ dissolved in 250 mL water and 155 mL KOH 1 M to maintain $Fe^{+3}/OH^- = 1/3$ ratio. KOH was added to adjust the pH to neutrality. The procedure ensures the formation of nano-particles of hydrated iron oxide (ferrihydrite poorly crystalline). The solid obtained was washed up to chloride negative reaction, centrifuged and then dried at 60 ºC. Activated minerals were identified adding the A letter to the mineral acronym (ZA, PA, KA and FCA, respectively).

Chemical analyses were performed by ICP-AES and ICP-MS (inductively coupled plasma mass spectrometry) for major elements and for arsenic**,** respectively (ALS Chemex Lab, Canada).

XRD (X-ray Diffraction) patterns were collected with a PHILIPS PW 1710 diffractometer using Cu Kα Ni-filtered radiation.

SEM-EDS (scanning electron microscopy and electron diffraction spectroscopy) measurements were performed in an ESEM (FEI Quanta 200), with tungsten filament and an ETD (high vacuum secondary electron) detector. Microanalysis was carried out with an EDAX Detector Apollo 40. Chemical results were expressed as w/w% oxides.

The BET surface area was measured by N_2 adsorption using a Micromeritics ASAP 2020 automated Braunauer Emmet-Teller Sorptometer.

Raman spectroscopic analyses were carried out on exhausted samples by means of inVia Renishaw Micro-Raman Spectrometer, equipped with an air-cooled CCD detector and edge filters. A 488.0 nm emission line from an Ar ion laser was focused on the sample by a Leica DLML microscope, using 5× or

20× objectives. The power of the incident beam is about 5 mW. Five 10 s accumulations were generally acquired for each sample. The resolution was 2 cm^{-1} and spectra were calibrated using the 520.5 cm^{-1} line of a silicon wafer. Data analysis included baseline removal and curve fitting, using a Gauss-Lorentz cross-product function by Peakfit 4.12 software (Jandel, AISN Software).

2.2 Arsenic Adsorption

Experiments were done following the adsorption method developed in our laboratory for Fe-rich clay as adsorbent [15]. The contact of the adsorbent material with arsenic containing solutions for set periods of time is followed by separation of the solids and by As determination in the supernatant solution. Additions of NaClO and APC (aluminum polychloride) are requested to ensure the arsenic oxidation (presence of arsenate(V) species) and to help the sedimentation process. The scheme of the process is shown in Fig. 1.

The arsenic solutions were prepared from a $Na_2HAsO_4 \cdot 7H_2O$ standard solution (1 g of arsenic L^{-1} of distilled water). The final pH was adjusted to 7 with NaOH 0.01 M. In order to maintain a relatively constant ionic strength, all arsenic solutions contained 0.01 M NaCl as background electrolyte.

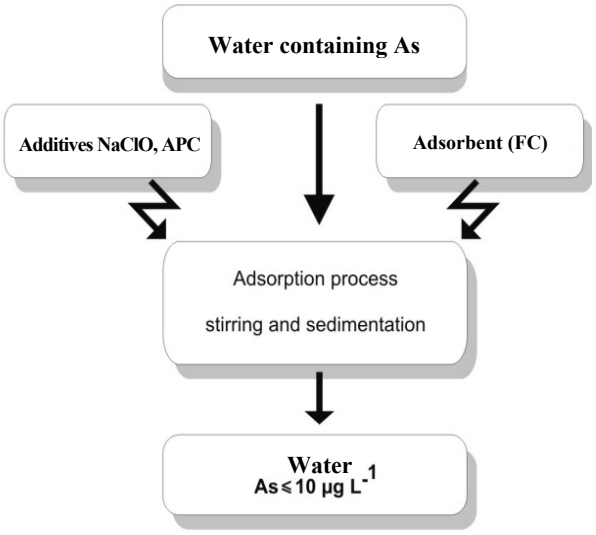

Fig. 1 Scheme of the arsenate removal method.

The batch experiments were carried out in a Jar test equipment (Velp) using adsorbent/water ratio = 1/10 (50 g aluminosilicate/0.5 L of water), pH 7 and room temperature (20 ± 2 ºC). The slurry was stirred during 60 min at 200 rpm to reach an optimal contact. Iron-poor raw materials (Z, P and K) as well as FC and the activated materials (ZA, PA, KA and FCA) were analyzed using water containing 200 µg of arsenic L^{-1}. In a preliminary step, batch experiments were carried out without the addition of coagulant to observe the behavior of the original minerals.

In a second step, the effective samples were tested with a solution containing 1000 $\mu g \cdot L^{-1}$ arsenic in order to determine the adsorbent saturation. The suspended solid was decanted with the aid of a small amount of APC (0.193 mg Al per liter of contaminated water). The material effectiveness was established through the number of useful consecutive treatment cycles. The adsorbent is considered saturated when the concentration of arsenic in the solution exceeds 10 $\mu g \cdot L^{-1}$ (limit established by the WHO).

The sedimentation with the APC addition occurs after 24 h without stirring. The turbidity of the supernatant liquid was measured using a Hanna turbidimeter. The accepted turbidity value was < 3 NTU. Arsenic was analyzed by a Perkin Elmer Analyst 200 (equipped with a Perkin Elmer HGA 900 graphite-furnace).

3. Results and Discussion

XRD patterns of raw materials are shown in Fig. 2. The predominance of 1:1 and 2:1 clays, K and P clays as well as Z were revealed. Main XRD lines are in agreement with PDF 80-0885, 46-1308 and 89-7539 respectively. The diffraction pattern of FC iron-rich clay, used as reference, showed the presence of P as dominant phase with small proportion of K, illite, hematite and quartz as associated species (PDF 46-1308, 80-0885, 26-0911, 85-0599 and 87-2096, respectively).

XRD-patterns of activated samples did not present

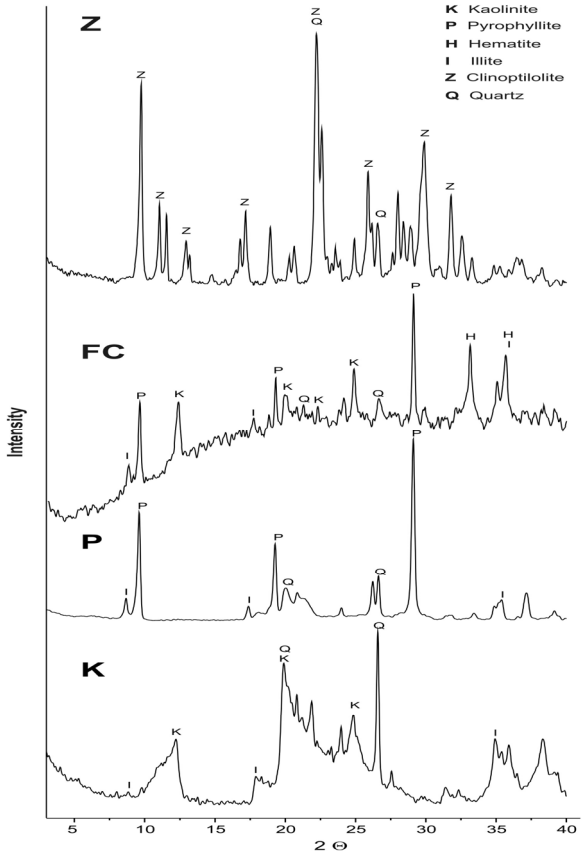

Fig. 2 XRD of studied samples.

variation respect to natural samples. This finding could be attributed to the small amount of added iron and/or to the low crystallinity of the iron phase. On the other hand, it is known that crystallization of iron oxides is affected by the presence of foreign species, in particular silicates. The Si-dissolution contributes to the formation and stability of poorly crystalline two-line ferrihydrite, preventing its transformation to crystalline Fe-O phases [17, 18].

Table 1 gives the ICP-AES chemical data for natural and iron-activated samples. After activation, the bulk iron content increase (expressed as w/w% of Fe_2O_3) was between 3%-5%. Slight diminution of the SiO_2 in some activated samples, particularly in the 2:1 clays, can be associated to the use of alkaline solution for iron activation; the silica dissolution is more effective in structures with high number of tetrahedral layers. The ICP-MS As values measured in natural species (expressed in ppm) are also included in Table 1. These values can be correlated with the iron content in the laminar materials. Comparatively, the zeolite clinoptilolite showed a higher proportion of arsenic in relation to the low content of iron.

EDS chemical data obtained for Fe_2O_3 both in natural and Fe-modified samples, Table 2 are slightly higher than the ICP-AES values reported in Table 1, revealing that the natural iron is deposited on the aluminosilicate surface. In natural samples the iron contents can be attributed to weathering processes of the proto-minerals, whereby the leaching leads to the dissolution and re-precipitation of iron oxides. An acceptable agreement between SiO_2/Al_2O_3 ratios determined by both methods is observed. The data can be compared with the theoretical values of 1.18, 2.35 and 5.8 for "ideal" pyrophyllite $Al_2(OH)_2Si_4O_{10}$, kaolinite $Al_2(OH)_4Si_2O_5$ and sodium clinoptilolite $Na_6Al_6Si_{30}O_{72}$ $20H_2O$, respectively.

BET specific surface area and APW (average pore width) for natural and Fe-modified samples are given in Table 3. With comparative purposes, the ferrihydrite synthesized according to the procedure [16] showed a BET surface area of 322.4 $m^2 \cdot g^{-1}$ and an APW of 28 Å. Natural samples have a surface area lower than that obtained for the activated samples. The increase is associated to the coating by fresh Fe(III)-oxide ferrihydrite-like phase. However, the surface behavior was not similar. The meso-porous size presented variations which can be attributed to several factors, in particular the characteristics of the surface where ferrihydrite is deposited (structure, presence of defects, substitutions, impurities, mineral associations, particle size, crystallinity and cation exchange in the case of zeolite). These factors affect also the iron distribution over the mineral particles with the generation of preferential sites, as seen in Fig. 3a, for the KA sample where the dispersion is inhomogeneous unlike that observed in PA (Fig. 3b).

Assuming that there are aluminosilicate-ferrihydrite mechanical associations, the total surface area can be estimated by the addition of the fractional amount of

Table 1 ICP-AES chemical analysis of major elements (in % w/w oxides) as by ICP-MS (in ppm).

%	FC	FCA	K	KA	P	PA	Z	ZA
SiO_2	21.10	17.38	51.92	49.57	67.10	63.71	62.74	60.60
Al_2O_3	15.66	13.43	32.32	30.85	26.39	25.87	12.51	12.04
Fe_2O_3	54.50	59.78	1.05	5.16	0.44	4.24	0.64	4.00
CaO	0.22	0.18	0.45	0.19	0.15	0.10	0.42	0.40
MgO	0.12	0.09	0.23	0.17	0.11	0.10	0.55	0.53
Na_2O	0.23	0.19	0.30	0.23	0.22	0.11	6.43	5.01
K_2O	1.40	1.66	0.20	0.63	0.11	0.21	1.53	1.79
Cr_2O_3	0.01	0.01	0.01	0.01	0.01	0.01	0.01	0.01
TiO_2	0.61	0.57	1.16	1.11	0.28	0.27	0.12	0.11
MnO	0.13	0.13	0.01	0.01	0.01	0.01	0.01	0.01
P_2O_5	0.29	0.25	0.05	0.07	0.04	0.09	0.01	0.01
SrO	0.06	0.06	0.01	0.01	0.01	0.01	0.15	0.15
BaO	0.07	0.08	0.02	0.01	0.01	0.01	0.04	0.04
LOI	5.60	6.19	12.27	11.98	5.12	5.26	14.84	15.30
As (ppm)	29.1	nd	1.8	nd	0.8	nd	6.2	nd
SiO_2/Al_2O_3	1.35	1.29	1.61	1.61	2.54	2.46	5.01	5.03

nd = not determined.

Table 2 Some EDS chemical data for natural and activated samples.

	FC	FCA	K	KA	P	PA	Z	ZA
% Fe_2O_3 (by EDS)	72.0	81.10	1.27	8.39	0.50	6.10	0.90	9.54
SiO_2/Al_2O_3 (by EDS)	1.36	1.30	1.59	1.57	2.48	2.40	4.96	4.95

Table 3 Surface properties of samples.

Sample	FC	FCA	K	KA	P	PA	Z	ZA
S_{BET} ($m^2 \cdot g^{-1}$)	12.4	24.5	9.1	23.6	7.7	30.1	9.5	35.9
APW (Å)	115.0	70.0	138.0	112.0	163.0	63.0	189.0	101.0
$S_{BET\ act}/S_{BET\ orig}$		1.9		2.6		3.9		3.7
S_{BET} activated samples Celis´expression ($m^2 \cdot g^{-1}$)		28.8		21.6		19.6		20.1

surface areas of each component, according to the Celis' expression [17]: $S_{total} = S_{mineral}\ (1 - x) + x\ S_{ferrihydrite}$, where S_{total} is the estimated specific surface area for the mixture while x is the fraction of ferrihydrite in the mineral-ferrihydrite mixture. The x value is calculated from the ICP chemical data. The estimated values are indicated in Table 3.

For the kaolinite, experimental and estimated BET-values are practically similar, unlike for the P and Z samples, for which experimental values are greater than these estimated for a physical mixture. Consequently, the surface characteristics of the iron deposited on the negatively charged basal planes of 2:1 clays and over the zeolite species are different respect to that observed for 1:1 clay. The inhomogeneous and multilayer adsorption observed in kaolinite reveals that the low porosity of ferrihydrite is not reflected in the resulting total BET, which resembles that of the raw material. For the other silicates, with higher exposition of tetrahedral layers, the Si dissolution increases. So, surfaces acquire negative charge. Consequently, the iron phase dispersion is more homogeneous, avoiding the aggregation process conducive to crystal particles. This effect can also contribute to the surface charge-inversion which ensures the attraction of the oxoanions [17, 19, 20]. In zeolite type species, the surface charge depends not only on the isomorphous replacement in the lattice but also on the cationic exchange capability. So, at the experimental pH, the electric properties and the

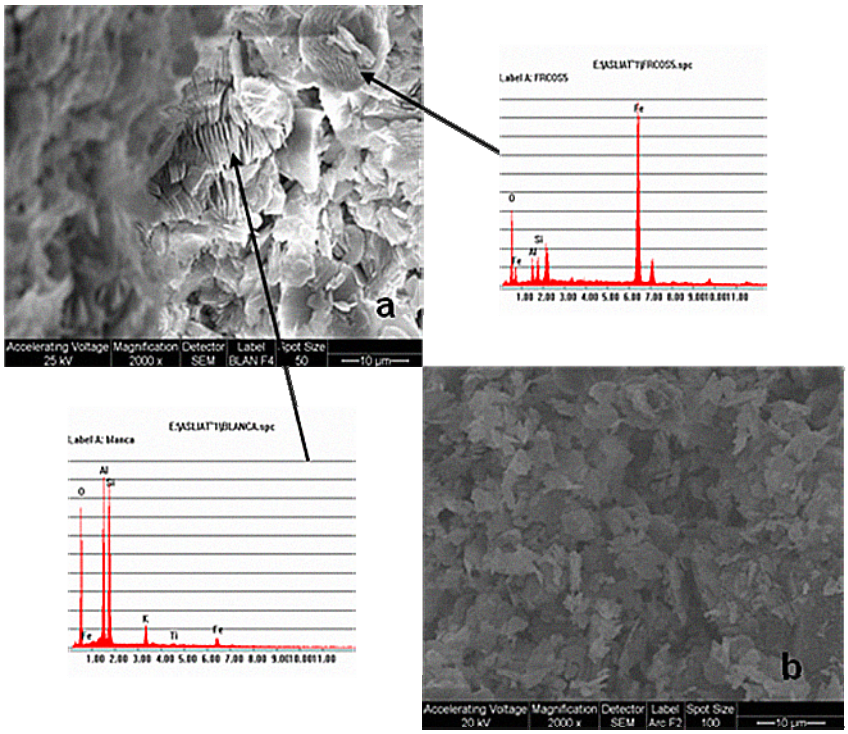

Fig. 3 Morphological properties of KA (a) and PA (b).

surface chemical reactivity can be affected.

On the other hand, for the natural Fe rich-clay, the estimated value of 28.8 $m^2 \cdot g^{-1}$ is higher than that experimentally observed. In this case, the presence of abundant hematite species, previously deposited in nature, blocks the aluminosilicate surface. The surface exposed to the chemical modification has a material with a PZC (point of zero charge) different from that observed in the other cases. In fact, the gap between the PZC of aluminosilicates and iron oxides is big (1-4 for the former and 7-9 for the last, respectively). So, the composition and structure of the raw material and the pH of the environment determine the iron adsorption capability. In this sense, it is reported that the maximum hematite formation from ferrihydrite occurs around neutral pH where the solubility is at a minimum and aggregation is a maximum. So, in the iron rich clay, the aggregated ferrihydrite increases the possibility of crystallization by a short-range process, which resembles to an epitaxial growth [18]. This fact is surely the reason for the lower value of BET surface of FCA sample, although the chemical activation involves similar iron values.

Results of preliminary experiments to remove arsenic with natural and Fe-activated samples, using water containing 200 $\mu g \cdot L^{-1}$ of As and without APC addition, given in Table 4, clearly indicate that only the FC sample is active. The other natural samples showed the arsenic leaching, originally present in the minerals. The interaction mechanism between arsenate and hydrous iron oxide phases has been ascribed to the formation of inner-sphere complexes between As (V) species (particularly AsO_4H^{2-}) and Fe(III)-OH or $-OH_2$ surface-groups [9].

The effectiveness of FC and Fe-activated samples (FCA, KA, PA and ZA) was evaluated through the number of treatment cycles up to adsorbent saturation. For these assays, water containing 1,000 $\mu g\ L^{-1}$ of As was used in the experimental conditions, including APC addition. Table 5 summarizes results, which are comparatively shown in Fig. 4.

The differences observed in the As removal performed for the various iron-activated samples can be attributed to their structural and compositional

Table 4 As content after one treatment cycle.

Sample	FC	FCA	K	KA	P	PA	Z	ZA
As ($\mu g \cdot L^{-1}$)	< 10	< 10	210	< 10	215	< 10	340	< 10

Table 5 Effectiveness of As adsorption (μg of As by g of adsorbent).

sample	Nº cycles	As adsorbed.
FC	45	445.50
FCA	70	693.00
KA	12	128.90
PA	27	277.70
ZA	17	178.10

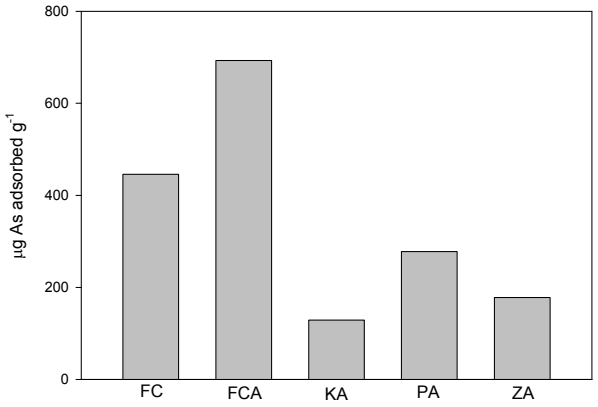

Fig. 4 As adsorbed for FC and activated samples.

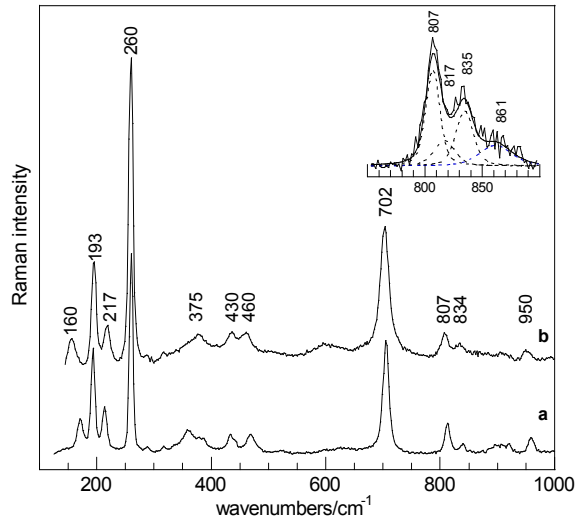

Fig. 5 Raman spectra of Fe-activated PA before (a) and after (b) As adsorption. Curve fitting results of curve b in the range 750-900 cm^{-1} are shown in the inset.

characteristics. The deposition of a similar content of hydrated iron oxide phase is comparatively more effective in 2:1 clays than in 1:1 kaolinite and zeolite, although the hematite presence in the FC must be also considered.

Direct evidence of As(V) species adsorption on activated samples is analyzed by Raman spectroscopy. Fig. 5 shows comparatively the Raman spectra of the PA (activated pyrophyllite) sample before (curve a) and after (curve b) As adsorption (27 cycles), respectively. Curve a closely resembles the spectrum typical of pyrophyllite (RRUFF database) with main peaks being at about 193, 260, 702, 810 and 957 cm^{-1}.

Although the identification of the vibrational modes of layered aluminosilicates is still open owing to the complexity of the structural unit, common features appear in the range 4,000-1,600 cm^{-1} (stretching and bending vibrations of water molecules) and below 1300 cm^{-1} (vibrations due to the silicate layer, OH bending and charge-balancing cations) [21, 22]. Weak bands in the region 800-1,100 cm^{-1} are attributed to Si-O stretching bond in SiO_4^{2-} tetrahedra whereas the strong peak around 700 cm^{-1} corresponds to the Si-O-Si vibrational modes connecting the SiO_4 tetrahedra in a layer. Al^{3+}-Fe^{3+}-OH and Fe^{3+}-Fe^{3+}-OH bending vibrations due to structural iron have been identified at about 907 cm^{-1} and between 800 cm^{-1} and 805 cm^{-1}, respectively [23]. The peaks in the region below 600 cm^{-1} arise from a complex set of translational motions of cations in octahedral sites and in interlayer sites, the strong peak at about 260 cm^{-1} is a common feature in most di-octahedral phyllosilicates [22]. On the other hand, the weak and broad Raman lines of ferrihydrite iron-oxide are centered in 370-380, 508-510 whereas the stronger band is located in 707-710 cm^{-1} [24]. So, the overlapping makes it difficult the assignation in activated samples.

After As adsorption the Raman spectrum (Fig. 5, curve b) exhibits similar band positions with a differentiation in the range 750-900 cm^{-1}. Besides, the band at 807 cm^{-1} typical of PA sample, curve fitting of

this spectral region (inset of Fig. 5) evidenced new components at 817 cm^{-1} and 861 cm^{-1} and an increase of the band intensity at 835 cm^{-1} attributed to the adsorbed As species. The band at 817 cm^{-1} can be assigned to the As-O symmetric stretching vibration of the $(AsO_4)^{3-}$ units whereas the band at 835 cm^{-1} and 861 cm^{-1} to As-O symmetric stretching in $HAsO_4^{2-}$ and $H_2AsO_4^{1-}$ surface species [25]. These findings suggest that arsenate species interact with iron oxy(hydroxides) sites forming inner-sphere bidentate or monodentate surface complexes or both in agreement with literature data.

Spectroscopic evidences and theoretical predictions agree with the view that As(V) adsorption occurs by complexation with iron oxy-hydroxide surfaces (ferrihydrite and goethite) preferentially yielding the formation of a bidentate complex [25-28] rather than a precipitated solid phase [24, 27].

4. Conclusions

The activation of natural iron-poor aluminosilicates such as Z as well as P and K clays by means of deposition of ferrihydrite-like species leads to materials with high capacity to interact with arsenate ions in the removal strategy, indicating that the chemical modification facilitates or enhances the arsenic removal capability. The arsenate adsorption, identified by Raman spectroscopy on the PA clay, occurred with the formation of inner-sphere surface complexes on the amorphous iron phase. The potentiality of these low cost mineral species, both originally with low or with a considerable iron content, strongly enhanced by small increase in the iron content (3%-5% as Fe_2O_3), can be attributed to their structural characteristics. Laminar 2:1 clays perform better than 1:1 kaolinite and zeolite, probably because of a more efficient spreading of the low symmetry iron oxyhydroxide ferrihydrite phase on their surface that improves the efficiency of activation and sorption process. So, chemical modification constitutes a simple, effective, accessible and eco-friendly technological alternative to prolong the lifetime of the Fe-rich adsorbent or increases the added-value of abundant and accessible iron-low aluminosilicates.

Acknowledgments

The work was done by financial support of ANPCyT PICT-2186 Argentina and CUIA Italy.

References

[1] A. Mukherjee, P. Bhattacharya, A. Fryar, Arsenic and other toxic elements in surface and groundwater systems, Applied Geochemistry 26 (2011) 415-420.

[2] H. Nicolli, J. Bundschuh, M. Blanco, O. Tujchneider, H. Panarello, C. Dapeña, et al., Arsenic and associated trace-elements in groundwater from the Chaco-Pampean plain, Argentina, Science of the Total Environment 429 (2012) 36-56.

[3] P. Smedley, D. Kinninburgh, A review of the source, distribution and behavior of arsenic in natural waters, Applied Geochemistry 17 (2002) 517-568.

[4] J. Bundschuh, P. Bhattacharya, D. Chandrasekharam, Remediation of arsenic-rich groundwater, in: Natural Arsenic in Groundwater: Occurrence, Remediation and Management, Taylor & Francis Group, London, 2005.

[5] A. Malik, Z. Khan, Q. Mahmood, S. Nasreen, Z. Bhatti, Perspectives of low cost arsenic remediation of drinking water in Pakistan and other countries, Journal of Hazardous Materials 168 (2009) 1-12.

[6] J. Bundschuh, P. Bhattacharya, O. Sracek, M. Mellano, A. Ramírez, A. Storniolo, et al., Arsenic removal from groundwater of the Chaco-Pampean Plain (Argentina) using natural geological materials as adsorbents, Part A, Journal of Environmental Science and Health 46 (2011) 1297-1310.

[7] D. Giles, M. Mohapatra, T. Issa, S. Anand, P. Singh, Iron and aluminium based adsorption strategies for removing arsenic from water, Journal of Environmental Management 92 (2011) 3011-3022.

[8] S. Aredes, B. Klein, M. Pawlik, The removal of arsenic from water using natural iron oxide minerals, Journal of Cleaner Production 29-30 (2012) 208-213.

[9] H. Guo, D. Stüben, Z. Berner, Q. Yu, Characteristics of arsenic adsorption from aqueous solution: Effect of arsenic species and natural adsorbents, Applied Geochemistry 24 (2009) 657-663.

[10] H. Altundogan, S. Altundogan, F. Tumen, M. Bildik, Arsenic removal from aqueous solutions by adsorption on red mud, Waste Management 20 (2000) 761-767.

[11] M. Vithanage, W. Senevirathna, R. Chandrajith, R.

Weerasooriya, Arsenic binding mechanisms on natural red earth: A potential substrate for pollution control, The Science of the Total Environment 379 (2007) 244-248.

[12] S. Maji, A. Pal, T. Pal, Arsenic removal from real-life groundwater by adsorption on laterite soil, Journal of Hazardous Materials 151 (2008) 811-820.

[13] Y. Mamindy-Pajany, Ch. Hurel, N. Marmier, M. Romeo, Arsenic adsorption onto hematite and goethite, Comptes Rendus Chimie 12 (2009) 876-881.

[14] Z. Li, W. Jiang, J. Jean, H. Hong, L. Liao, G. Lv, Combination of hydrous iron oxide precipitation with zeolite filtration to remove arsenic from contaminated water, Desalination 280 (2011) 203-207.

[15] E. Soto, M. Gonzalez, H. Thomas, I. Schalamuk, I. Botto, Arsenic removal from groundwater: Technological design for rural areas, Augmdomus 5 (2013) 109-119.

[16] U. Schwertmann, R. Cornell, Iron Oxides in the Laboratory: Preparation and Characterization, 2nd ed., Wiley-Vch, Weinheim, Germany, 2000.

[17] R. Celis, J. Cornejo, M. Hermosin, Textural properties of synthetic clay-ferrihydrite associations, Clay Minerals 33 (1998) 395-407.

[18] R. Cornell, U. Schwertmann, The Iron Oxides: Structure, Properties, Reactions, Occurrences and Uses, 2nd ed., Wiley-Vch, Weinheim, Germany, 2006, pp. 393-394.

[19] J. Oades, Interactions of polycations of aluminum and iron with clays, Clay and Clay Minerals 32 (1984) 49-57.

[20] M. Arias, M. Barral, F. Diaz-Fierros, Effects of iron and aluminium oxides on the colloidal and surface properties of kaolin, Clays and Clay Minerals 43 (1995) 406-416.

[21] Y. Huang, Z. Jiang, W. Schwieger, Vibrational spectroscopic studies of layered silicates, Chemisry of Materials 11 (1999) 1210-1217.

[22] A. Wang, J. Freeman, K. Kuebler, Raman spectroscopic characterization of phyllosilicates, Lunar and Planetary Science 33 (2002) 1374.

[23] S. Lantenois, J. Bény, F. Muller, R. Champallier, Integration of iron in natural and synthetic Al-pyrophyllites: An infrared spectroscopic study, Clay Minerals 42 (2007) 129-143.

[24] S. Das, M. Hendry, Application of Raman spectroscopy to identify iron minerals commonly found in mine wastes, Chemical Geology 290 (2011) 101-108.

[25] K. Müller, V. Ciminelli, M. Dantas, S. Willscher, A comparative study of As(III) and As(V) in aqueous solutions and adsorbed on iron oxy-hydroxides by Raman spectroscopy, Water Research 44 (2010) 5660-5672.

[26] S. Myneni, S. Traina, G. Waychunas, T. Logan, Experimental and theoretical vibrational spectroscopic evaluation of arsenate coordination in aqueous solutions, solids and at mineral-water interfaces, Geochimica and Cosmochimica Acta 62 (1998) 3285-3300.

[27] S. Goldberg, C. Johnston, Mechanisms of arsenic adsorption on amorphous oxides evaluated using macroscopic measurements, vibrational spectroscopy and surface complexation modeling, Journal of Colloid and Interface Science 234 (2001) 204-216.

[28] Y. Jia, L. Xu, Z. Fang, G. Demopoulos, Observation of surface precipitation of arsenate on ferrihydrite, Environmental Science and Technology 40 (2006) 3248-3253.